Applied Catalysis B: Environmental 119–120 (2012) 217–226

Contents lists available at SciVerse ScienceDirect

Applied Catalysis B: Environmental

journal homepage: www.elsevier.com/locate/apcatb

Highly stable ytterbium promoted Ni/γ-Al_2O_3 catalysts for carbon dioxide reforming of methane

Mohamad Hassan Amin, Kshudiram Mantri, Jarrod Newnham, James Tardio, Suresh K. Bhargava*

Advanced Materials & Industrial Chemistry Group, School of Applied Sciences, RMIT University, Melbourne, VIC 3001, Australia

ARTICLE INFO

Article history:
Received 10 November 2011
Received in revised form 27 February 2012
Accepted 29 February 2012
Available online 10 March 2012

Keywords:
CO_2 reforming of methane
Yb/Ni/γ-Al_2O_3
Syngas

ABSTRACT

The influence of Yb on Ni(20 wt%)/γ-Al_2O_3 catalysts (prepared via a sol–gel method) for use in the dry reforming of methane was investigated. It was found that the addition of low quantities of Yb (1–2 wt%) led to significant increases in catalytic activity and catalyst stability, and the production of H_2 and CO at a ratio close to unity (~0.95). Higher levels of Yb doping (3–8 wt%) did not achieve similar increases in activity as those observed in the lower level doped catalysts. Based on characterisation studies conducted on the catalysts before and after testing it was found that the catalyst with a low level of Yb (2 wt%) had the smallest average Ni particle size, narrowest particle size distribution and highest ease of reducibility (based on Temperature Programmed Reduction analysis). Analysis of the catalysts after testing showed that the catalyst with 2 wt% Yb also experienced the lowest level of carbon deposition and contained a high degree of graphitised carbon. The results obtained indicate that doping of Ni-Al_2O_3 catalysts with a select amount of Yb can give rise to a catalyst with excellent properties for use in the dry reforming of methane and that Yb can have a significant role in controlling the size/mobility of Ni nanoparticles produced via reduction of NiO.

1. Introduction

Global concern about increasing anthropogenic CO_2 emissions has led to increased interest in processes that can utilise carbon dioxide as a feedstock. CO_2/dry reforming of methane (DRM, Eq. (1)) is a promising process that could potentially be used to convert CO_2, from concentrated carbon dioxide waste streams, into a valuable product, syngas, which is the basic building block for many valuable chemicals [1]. In comparison to conventional steam reforming or partial oxidation of methane, DRM is more appropriate in remote natural gas or crude oil fields, where water supplies are limited [2]. Moreover it results in "CO-richer" synthesis gas with a relatively low H_2/CO ratio, which is more desirable for the direct use as feedstock for carbonylation, hydroformylation, Fischer–Tropsch synthesis of long chain hydrocarbons and direct production of dimethyl ether (DME) [1,2].

$$CH_{4(g)} + CO_{2(g)} \leftrightarrow 2CO_{(g)} + 2H_{2(g)} \quad \Delta H_{973} = 260\,\text{kJ/mol} \qquad (1)$$

In recent years the main aim of research on CO_2 reforming of methane has been the development of improved materials for catalysing this reaction. Of the numerous catalysts that have been investigated the most successful to date include noble metal (Pt, Pd, Rh, Ru) supported catalysts and Ni based catalysts. Ni based catalysts in particular have received considerable attention due to their lower cost and similar activity and selectivity compared to the noble metal supported catalysts. Ni-based catalysts however have a larger tendency to undergo deactivation via carbon deposition and sintering hence significant efforts have been devoted to improvements in the aforementioned areas [3–5]. There have also been recent efforts focussed on gaining a better understanding of the carbon deposition that occurs which led to findings that show there are a number of different types of carbon that may be deposited during catalysed dry reforming of methane. The deposited carbon can have different structural order, depending on the specific reaction conditions and size and structure of the catalysts active sites [1,2,6,7]. The types of carbon that can form include atomic carbon, amorphous carbon, bulk carbide, whisker, encapsulating, filamentous and carbon nanotubes [6–9].

Approaches to achieve improvements in the activity and stability of Ni based catalysts for the dry reforming of methane have focussed mostly on the discovery of suitable promoters/Ni based bi-metallic catalysts [10–15] and the discovery of better supports [12,13]. The types of promoters for Ni based catalysts that have been studied include alkali [11,16], alkaline earth [16–18], transition metal [16,19] and rare earth metal oxides [20–22]. A number of these studies have also been conducted on Ni based catalysts containing multiple metals/oxides from different groups.

* Corresponding author. Tel.: +61 3 9925 3365; fax: +61 3 9925 3747.
E-mail address: suresh.bhargava@rmit.edu.au (S.K. Bhargava).

0926-3373/$ – see front matter © 2012 Elsevier B.V. All rights reserved.
doi:10.1016/j.apcatb.2012.02.039

Transition metals that have been investigated as promoters in Ni-based dry reforming catalysts include Au [9], Mn [10,16,23–26], Ti [26], Cu [27,28], Co [28–30], V [31], Fe [28], Mo [32], Zr [2,19,33,34], Pt [3,35–37], Rh [37–39] and Pd [37]. Some authors reported a negative effect on the catalytic performance over nickel catalysts modified by Au [9], Sn [16], Ag [16], Mn [16,27], Fe [28], Cu [28] and Ti [26] whilst others reported some positive effects. Fan et al. [30] reported that the addition of Co to a Ni/MgO-ZrO_2 catalyst improved its activity due to the stabilisation of the t-phase in zirconia, better metal dispersion, small metal particle size and synergetic effect between Ni and Co particles. Chen et al. [27] reported that the addition of Cu to their Ni catalyst led to stabilisation of the structure of the active sites on the Ni surface for the methane cracking reaction. Chen et al. [27] reported that this stabilisation led to improved regeneration through preventing the deactivation of the Ni catalyst which can be caused by sintering or by loss of nickel crystallites. A beneficial effect of vanadium on methane conversion was observed over a Ni/Al_2O_3 catalyst by Valentini et al. [31]. They stated that this was due to avoiding the formation of the aluminate spinel phase. Liu et al. [26] studied the effect of promoting a Ni-MCM-41 catalyst with Mn, Zr, Ti and Zn and found that the addition of Zr to Ni-MCM-41 led to significant improvements in the activity and long term stability of this Ni based catalyst. These improvements were attributed to Zr enhancing the structural stability and dispersion of active nickel sites whilst also having a strong anchoring effect and involvement in partial oxidation of CO_2.

Alkali and alkaline earth metals that have been investigated in the promotion of Ni-based dry reforming catalysts include Li [11], K [10,11,16,24,40–44], Ca [12,16,24,40,41,45] and Mg [12,17,24,40]. It was reported that the introduction of 0.5 wt% of the metals K and Li on Ni/Al_2O_3 and Ni/CeO_2 catalysts reduced coke deposition but decreased reactant conversions and the H_2/CO ratio of the products. The authors suggested that this result could have been a consequence of the blockage of Ni active sites by the alkaline metals or due to methane cracking and the enhancement of carbon gasification [11,16,45]. It has been reported that addition of Ca to a Ni/Al_2O_3 catalyst caused a dramatic reduction of catalytic activity and a significant increase in carbon deposition [16]. This was apparently due to carbon deposition occurring through the deposition of a paraffin polymeric –CH_2– chain, which is slowly transformed into a less reactive polyaromatic deposit, which tends to form graphite [16]. Dias and Assaf [46] reported that calcium added to a Ni/Al_2O_3 catalyst interacted with the support and lowered its resistance to sintering. It was reported that the addition of Mg reduced the size of Ni species and produced highly dispersed Ni species, and consequently, retarded the sintering of nickel species on the catalyst surface in a Ni-Mg/HY catalyst [24].

Some rare earth oxides have been used as promoters in Ni based catalysts for the dry reforming of methane, with Ce, La and Pr oxides being the most widely studied [7,9,20–22,47–52]. It was reported that the addition of CeO_2 effectively promotes Ni metal dispersion on the surface of Al_2O_3 catalysts despite undesirable self-dispersion of the CeO_2 promoter [20,47–50,53]. The addition of La_2O_3 and CeO_2 as promoters also showed other beneficial effects on the catalyst performance, such as the suppression in the sintering of Ni particles and delaying the transition of the alumina support from γ-Al_2O_3 to low-surface-area phase α-Al_2O_3 [20,22]. These promoters have also been shown to: induce formation of reactive filamentous carbon on Ni-based catalysts; promote CO_2 adsorption on the surface of the catalyst [49], affect the chemical environment and electronic state of Ni at the Ni–REO interface [51]; and reduce the chemical interaction between nickel and the support resulting in an increase in reducibility and stronger dispersion of nickel [54]. Of the studies conducted that utilised CeO_2 as a sole or co-promoter Wang and Lu found an optimum weight loading of 1–5 wt% CeO_2 on a Ni/γ-Al_2O_3 catalyst [50], whilst Laosiripojana et al. reported that 8% ceria on the same support gave a maximum in activity [48]. Pompeo et al. in 2009 showed that a Ni catalyst supported on Ce–Zr–α-Al_2O_3 composites present reforming activity and stability noticeably higher than in the case of the Ni catalyst supported on commercial α-Al_2O_3 [22]. Of the studies conducted that utilised La_2O_3 as a promoter Liu and co-workers reported that the addition of La_2O_3 improved the activity of Ni/θ-Al_2O_3 and Ni/La_2O_3/Al_2O_3 catalyst had an optimum amount of La_2O_3 loading with a La/Al/ratio of 0.05 with the highest activity and stability [7]. Zhang et al. reported that the amount of carbon deposition on the La_2NiO_4/ZSM-5 catalyst was smaller than the amount on the Ni/ZSM-5 zeolite catalyst [49].

Of the different types of elements/oxides that have been used as promoters in Ni-based dry reforming catalysts, the rare earth oxides have not been studied extensively (with some elements from this group having not previously reported on in the literature as promoters for Ni-based dry reforming catalysts). One of the rare earth elements that has not been studied previously, Yb, was selected for the detailed studies that are reported on here. These detailed studies were conducted based on some excellent preliminary results that were recently obtained using Yb as a promoter for a Ni/Al_2O_3 catalyst used in the dry reforming of methane [55]. The main aims of these studies were to determine the influence of varying amounts of Yb on the properties of Ni/Al_2O_3 catalysts, such as surface area and Ni particle size and morphology.

2. Materials and methods

2.1. Catalyst preparation

Ni(20 wt%)/γ-Al_2O_3 containing varying amounts of Yb (1–8 wt%) were prepared using a sol–gel method. In a typical synthesis, 32.06 g of aluminium isopropoxide (Aldrich) was hydrolysed with 250 mL of deionised water containing 1.5 wt% nitric acid at 80 °C for 3 h with vigorous stirring. This led to the generation of a clear boehmite sol. Separately, 6.23 g of $Ni(NO_3)_2{\cdot}6H_2O$ (Aldrich) and pre-determined amounts of ytterbium nitrate (Aldrich) were added to the boehmite gel. The resulting co gel was allowed to stand (unstirred) at room temperature in a beaker for 48 h to allow the solvent to evaporate. Finally, the dry co gels were calcined at 800 °C, for 6 h under static air. Hereafter these materials are referred to as Ni-*x*Yb/γ-Al_2O_3 (*x* = 0, 1, 2, 3, 4, 6, 8 wt%). The reference sample NiO was also prepared by the same procedure. For comparison purposes, 8 wt% Yb was loaded to Ni-0Yb/γ-Al_2O_3 sol–gel prepared powder using a wet impregnation method. This involved exposing commercial Yb_2O_3 (Merck) to an aqueous suspension of Ni-0Yb/γ-Al_2O_3 sol–gel prepared powder under vigorous stirring before calcination.

2.2. Characterisation

The materials were characterised for BET surface area (Micromeritics ASAP 2010), crystalline phases (powder XRD, Bruker D8 Advance X-ray diffractometer), surface element composition (Thermo Scientific K-Alpha XPS spectrometer), morphology and texture (transmission electron microscopy, JEOL 1010 TEM). Spent catalysts were characterised by XRD, TEM, Thermogravimetric Analysis (TGA) (Perkin-Elmer TGA 7) and FT-Raman (Perkin Elmer-Raman Station 400F). To determine the absolute peak positions in XPS, the C1s peak arising from the hydrocarbons adsorbed from the residual gas onto the pure γ-alumina and Ni/γ-Al_2O_3 were used for calibration. The energy of the C1s level arising from the pure γ-alumina and Ni/γ-Al_2O_3 was 285.0 eV. The temperature-programmed reduction (TPR) of the calcined catalysts was undertaken in a quartz reactor (I.D. 4.5 mm), packed with 50 mg

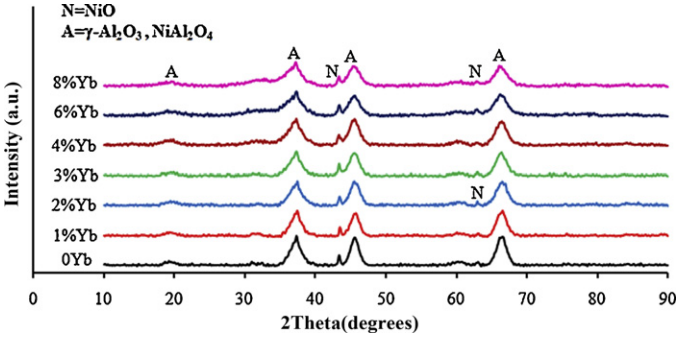

Fig. 1. XRD patterns of non-doped and Yb-promoted Ni/γ-Al_2O_3 sol–gel prepared catalysts.

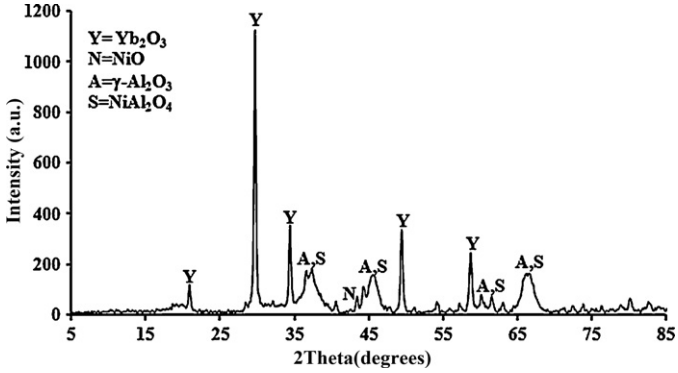

Fig. 2. XRD pattern of a mixture of 8 wt%Yb and Ni/γ-Al_2O_3 sol–gel prepared catalyst.

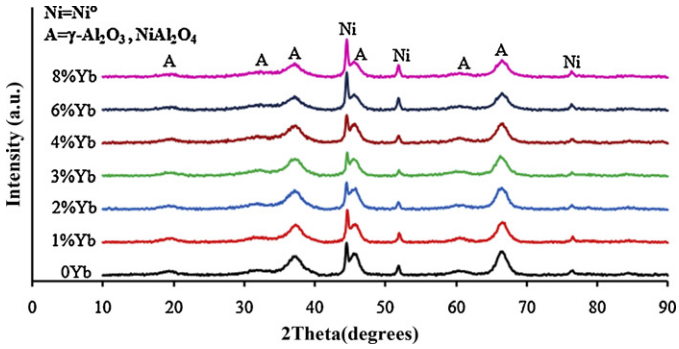

Fig. 3. XRD patterns of non-promoted and Yb-promoted Ni/γ-Al_2O_3 sol–gel prepared catalysts (reduced at 700 °C under H_2 flow).

catalyst in a flow (20 mL min^{-1}) of H_2–Ar mixture (4.14 mol% H_2) from 250 °C to 880 °C at a linear heating rate of 10 °C min^{-1}. The H_2 consumed in the TPR study was measured quantitatively by TCD. Before the TPR study, the catalyst was pretreated at 500 °C for 1 h under a flow (20 cm^3 min^{-1}) of argon.

2.3. Catalyst testing

The CO_2 reforming of methane was carried out at 700 °C in a fixed-bed continuous flow quartz reactor at atmospheric pressure and a gas hourly space velocity (GHSV) of 5.2×10^4 mL g^{-1} h^{-1}. The aforementioned reaction parameters were used in all tests unless stated otherwise. The catalyst was pre-reduced in situ in a mixed flow of H_2 and He (10:40 mL min^{-1}) at 700 °C for 2 h. The reactant gases (CO_2 and CH_4) were then fed (CO_2:CH_4:He = 1:1:2 mL min^{-1}) into the reactor. The product gas mixture was analysed by on-line gas chromatography (Shimadzu GC, 17A) equipped with a silica packed column and a TCD. The time-on-stream activity and durability of the catalysts were carried out at 700 °C for 20 h. After the durability test, the catalyst was removed and TGA was used to analyse the amount of deposited carbon.

The effects of feed flow rate (gas film thickness) and catalyst particle size on reaction rate were determined experimentally with a feed mixture composed of CO_2:CH_4:He (=22:22:44 vol.%) at 700 °C. It was seen that methane conversion was independent of the average size of the particles, within the particle size range of 500–710 μm so the internal mass transfer limitations do not occur under the conditions applied. In addition, the influence of external diffusion limitations was investigated by measuring the activity as a function of the catalyst loading at constant W/F (W = catalyst mass, F = total flow of feed gas). The conversion was not affected by changing the amount of catalyst and the flow, i.e. at constant contact time. Thus, external mass transfer limitations do not occur under the conditions applied.

3. Results

3.1. Characterisation

XRD patterns of the prepared materials, prior to being reduced, are shown in Fig. 1. The XRD patterns of all the materials consisted of the characteristic diffractions lines for γ-Al_2O_3 (and/or $NiAl_2O_4$) and NiO phases. Interestingly diffraction lines that would have indicated the presence of Yb_2O_3 were not detected even for the material with the highest Yb loading of 8 wt%. The lack of diffraction lines for Yb_2O_3 in the prepared materials (particularly the materials with high Yb loading) was investigated further by conducting XRD analysis of a mixture of Yb_2O_3 and γ-Al_2O_3 that contained 8 wt% Yb (Fig. 2). The diffraction pattern obtained for this mixture showed that if the Yb in the prepared materials was in the form of crystalline Yb_2O_3 it would clearly be detected at the loadings used. Hence the Yb in the Yb doped Ni catalyst was clearly not in the form of crystalline Yb_2O_3 and most likely present as either amorphous Yb_2O_3 (and/or as part of another amorphous phase), or in a highly dispersed form that could not be detected using XRD.

The XRD patterns obtained for the non-doped and Yb doped materials after being reduced under similar conditions to those used at the beginning of catalyst testing (in a mixed flow of H_2 and He at 700 °C for 2 h) are presented in Fig. 3. It can be seen from these patterns that after the reducing treatment the samples do not show any peaks for NiO. Well resolved peaks can be observed at 2θ values of ~44.6°, ~51.9° and ~76.5°, which correspond to the (1 1 1), (2 0 0) and (2 2 0) planes of Ni^0. Again no diffraction lines due to Yb based compound(s) were observed in all of the materials studied. The NiO (in the pre-reduced catalysts) and Ni^0 (in the reduced catalysts) average particle diameters calculated based on the peak broadening of the NiO (0 1 2) and Ni (1 1 1) diffraction peaks using the Scherrer formula are given in Table 1. The average particle diameter for NiO was in the range of 15.6 nm to 26.6 nm and was found to increase slightly with increasing Yb loading. The same trend however was not observed for the Ni^0 particles in the reduced catalysts with the catalyst containing 2 wt% Yb having a smaller (11.5 nm) average particle size than the catalyst with no Yb. The 2 wt% Yb loaded catalyst also showed the highest

Table 1
Particle size of nickel species in non-reduced and reduced Ni/γ-Al_2O_3 catalysts with different Yb loading (nm).[a]

Yb load (wt%)	0	2	4	6	8
NiO (non-reduced catalysts)	15.6	16.2	18.1	21.3	26.6
Ni^0 (reduced catalysts)	15.9	11.5	15.3	17.9	21.7

[a] Measured by X-ray diffraction line broadening method and Scherrer formula.

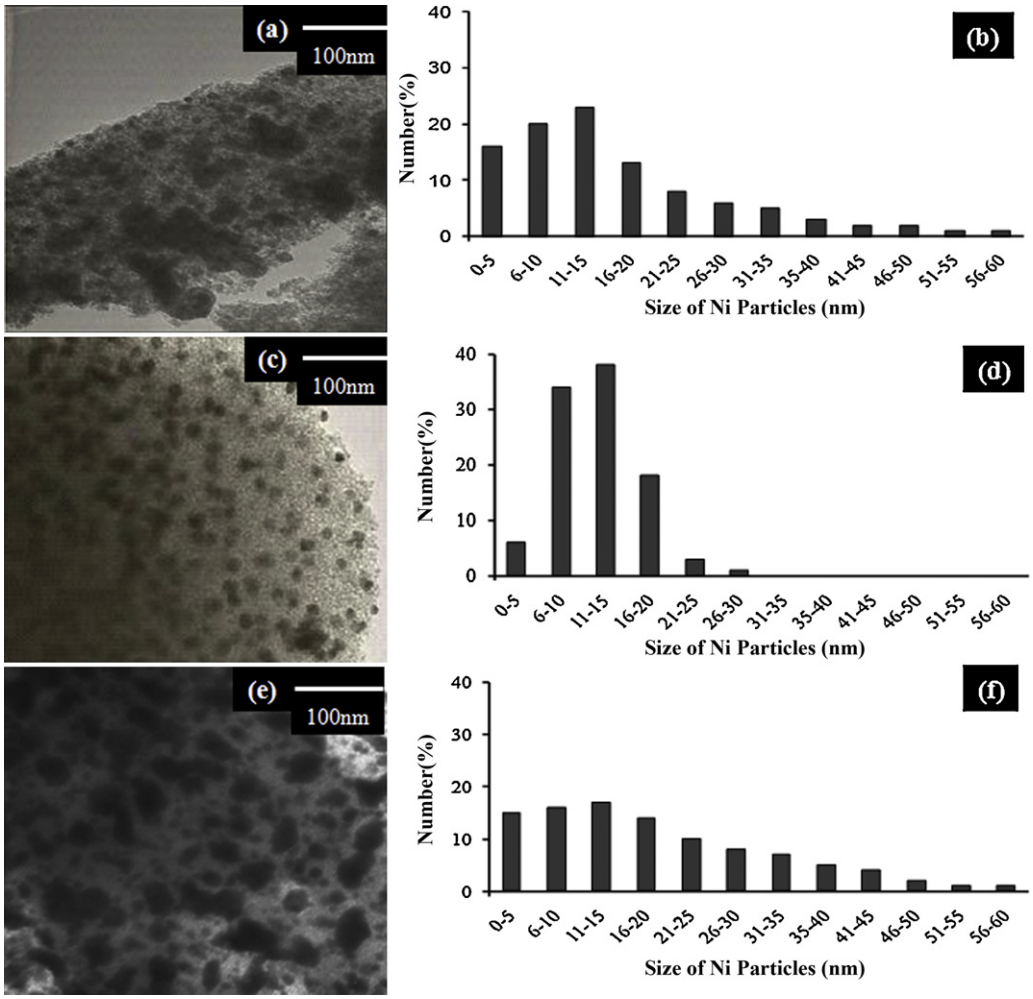

Fig. 4. Transmission electron micrographs and Ni particle size distribution of reduced catalysts (a, d) Ni/γ-Al_2O_3, (b, e) Ni-2Yb/γ-Al_2O_3 and (c, f) Ni-8Yb/γ-Al_2O_3.

shrinkage (∼5 nm) in ($NiO \rightarrow Ni^0$) particle size after reduction, whereas the undoped Ni/γ-Al_2O_3 showed an increase in ($NiO \rightarrow Ni^0$) particle size after reduction (∼2%) indicating that Yb had an influential role in stabilising the Ni particle size during the reducing treatment step.

Fig. 4 shows TEM images and Ni particle size distribution of reduced Ni/γ-Al_2O_3 with (2 and 8 wt% Yb) and without Yb. It is clear from the images that the Ni^0 particles in the 2 wt% Yb loaded catalyst are more dispersed and smaller in average size in comparison with the Ni^0 particles in the catalyst that did not contain Yb. The average size of the Ni^0 particles in the aforementioned catalysts as observed from the TEM images were in good agreement with the average sizes that were determined using the XRD data. The 2Yb-Ni/γ-Al_2O_3 catalyst had a more homogeneous particle size distribution than both the undoped and the 8% Yb doped catalysts. The particle size distributions obtained shows that the portion of smallest particles (0–5 nm) as well as the portion of largest particles (>30 nm) is higher for undoped and high Yb loaded Ni/γ-Al_2O_3 catalysts. The particle size distribution results observed for the 2Yb-Ni/γ-Al_2O_3 catalyst are consistent with results from previous studies that have shown that the addition of rare earth metals including La [56], Ce [57] and Pr [58] can prevent transition metals from agglomerating and sintering.

The BET surface area, pore size and pore volume of the Yb-promoted Ni/γ-Al_2O_3 catalysts are given in Table 2. From the data given in Table 2 it can be seen that the surface area of the catalysts increased slightly with increasing Yb doping. This increase was most likely due to a combination of the following. Firstly the added Yb in these materials did not cause significant pore blockage and secondly the added Yb most likely slightly increased the thermal stability of the materials, which in turn led to a reduction in the break down of the materials during the calcination step. Similar increases in thermal stability due to the addition of rare earth promoters have been reported previously [48,50,59,60].

The surface composition of the reduced Ni/γ-Al_2O_3 materials, with respect to Ni, was determined using XPS (Table 3). The

Table 2
Characteristic properties of Ni/γ-Al_2O_3 catalysts with different Yb loading.

Yb load (wt%)	0	2	4	6	8
BET surface area ($m^2\ g^{-1}$)	123	127	128	130	125
Average pore radius (nm)[a]	7.788	7.559	7.300	6.592	6.938
Average pore volume ($cm^3\ g^{-1}$)[b]	0.239	0.239	0.232	0.215	0.217

[a] Average of adsorption and desorption average pore diameter (4 V/A by BET).
[b] Average of adsorption and desorption single point total pore volume of pores.

Table 3
% Nickel in surface of reduced Ni/γ-Al_2O_3 catalysts with different Yb loading as determined by XPS.

Yb load (wt%)	0	2	4	6	8
Nickel in surface (atom%)	21.04	20.61	20.11	15.86	1.74

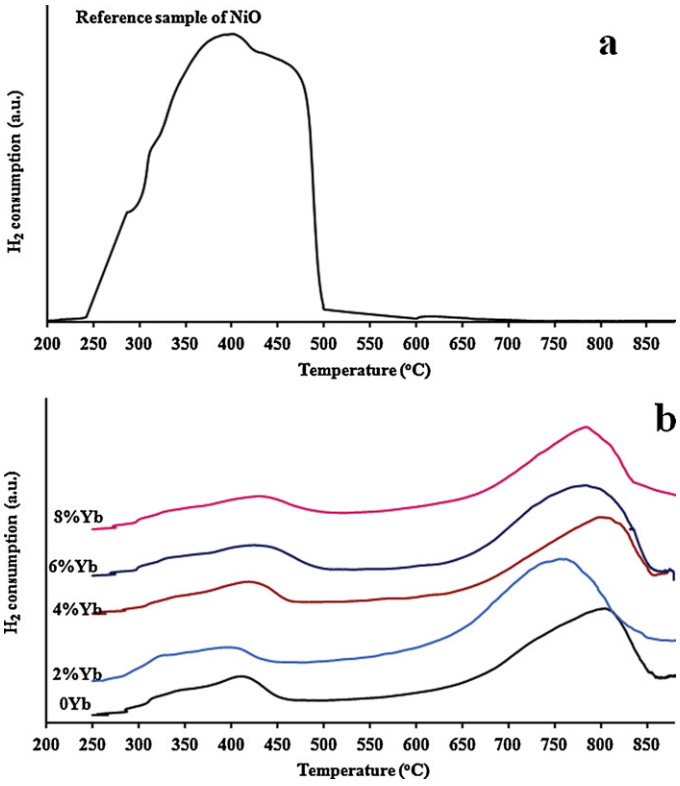

Fig. 5. TPR profile of (a) NiO and (b) Yb-promoted Ni/γ-Al_2O_3 catalysts.

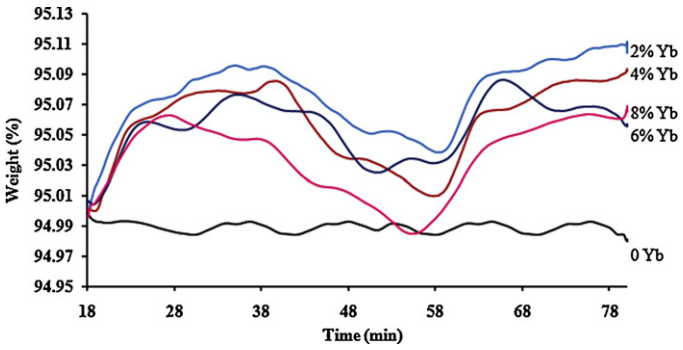

Fig. 6. Weight change of pure and Yb-promoted Ni/γ-Al_2O_3 sol–gel prepared catalysts (non-reduced) during nitrogen → oxygen → nitrogen → oxygen cycles at 700 °C.

contribution of Ni to the surface composition was found to decrease with increasing Yb loading. The extent of this decrease however was not significant at an Yb loading of 2 wt% where the % Ni in the surface of this material was only marginally lower than the material with no Yb. The decrease in Ni in the surface of the material containing 8 wt% Yb was however substantial. This was most likely due to the Yb present forming a surface layer predominantly on the Ni particles. This behaviour is similar to that reported by Daza et al. [52], where it was found that the use of high amounts of Ce in Ni-Mg-Al catalysts formed surface coatings on the Ni sites and reduced the superficial area of the solid.

The reducibility of the non-promoted and Yb-promoted Ni/γ-Al_2O_3 catalysts were studied using TPR. Fig. 5 shows the TPR profiles of the catalysts and a non-supported NiO for comparison. The TPR profile for NiO shows that reduction of the Ni started at ~240 °C and reached a maximum rate at ~400 °C. The TPR profiles of all the catalysts consisted of two clear reduction temperature zones. The low temperature zone (270–490 °C) and a high temperature zone (600–850 °C) represent the reduction of NiO and non-stoichiometric nickel aluminate in Ni/γ-Al_2O_3 respectively [7,61]. Based on the amount of H_2 consumed in the two temperature zones the majority of the oxidised Ni in both the non-doped and Yb doped materials was present in the form of a non-stoichiometric nickel aluminate. From the TPR profiles presented in Fig. 6 it can be seen that Yb doping did not have a similar effect on the temperatures at which the maximum rates of Ni reduction occurred for the four Yb doped materials. Of these materials the material containing 2 wt% Yb clearly had a significantly lower temperature for maximum Ni reduction for the Ni present in the form of a non-stoichiometric aluminate. The reduction of Ni in the NiO particles on this particular catalyst was also slightly higher at lower temperatures than that observed for the non-doped and other Yb doped materials.

Based on the H_2 consumption obtained from TPR analysis the reducibility of calcined samples was calculated as shown in Table 4. The reducibility of NiO/γ-Al_2O_3, which was used as the reference material, was defined as 1. The addition of 2 wt% Yb clearly made the Ni/γ-Al_2O_3 catalyst more reducible (which was most likely due to the added Yb leading to the formation of a decreased extent of stoichiometric $NiAl_2O_4$ spinel, which is difficult to reduce) [62].

Li et al. [62] reported that the addition of CeO_2 makes oxygen atoms connecting with Ni in the oxide catalysts more reactive and results in a high reducibility of NiO in Ni/Al_2O_3-ZrO_2-CeO_2. As this type of influence may have also been applicable to the reducibility of NiO in the catalyst precursor (from the added Yb_2O_3 present) it was decided to investigate the oxygen storage/adsorption characteristics of the non-doped and Yb doped Ni/γ-Al_2O_3 materials. This was investigated by monitoring the weight change of these materials in the presence of alternating gas environments (oxygen and nitrogen) at 700 °C (Fig. 6). For the Yb-promoted catalysts, it can be observed that when the gas flow was switched from nitrogen to oxygen the weight of the materials started to increase with time, but for the un-doped catalyst there was no significant weight variation. The weight of the Yb-promoted samples also decreased when the flow was switched back to nitrogen. The weight change in the experiments with the Yb-promoted catalysts is associated to the oxygen transport in or out of the oxide structure, which may be involved in the oxidation–reduction processes. The above result suggests that ytterbium oxides have a facility to reoxidise, and consequently it may interact with NiO to form YbO_2 and Ni^0.

3.2. Catalytic activity for dry reforming of methane

The ability of the un-doped and Yb doped Ni/γ-Al_2O_3 materials to catalyse the dry reforming of methane was investigated at 700 °C using a GHSV of 5.2×10^4 mL g^{-1} h^{-1} for a period of

Table 4
Reducibility of Ni/γ-Al_2O_3 catalysts with different Yb loading.

Yb load (wt%)	0	2	4	6	8
Temperature of the first peak (°C)	410	396	418	426	430
Reduction degree of the first peak	0.16	0.21	0.13	0.13	0.21
Temperature of the second peak (°C)	804	762	800	784	784
Reduction degree the second peak	0.52	0.74	0.42	0.34	0.46
Total reduction degree	0.68	0.95	0.55	0.47	0.67

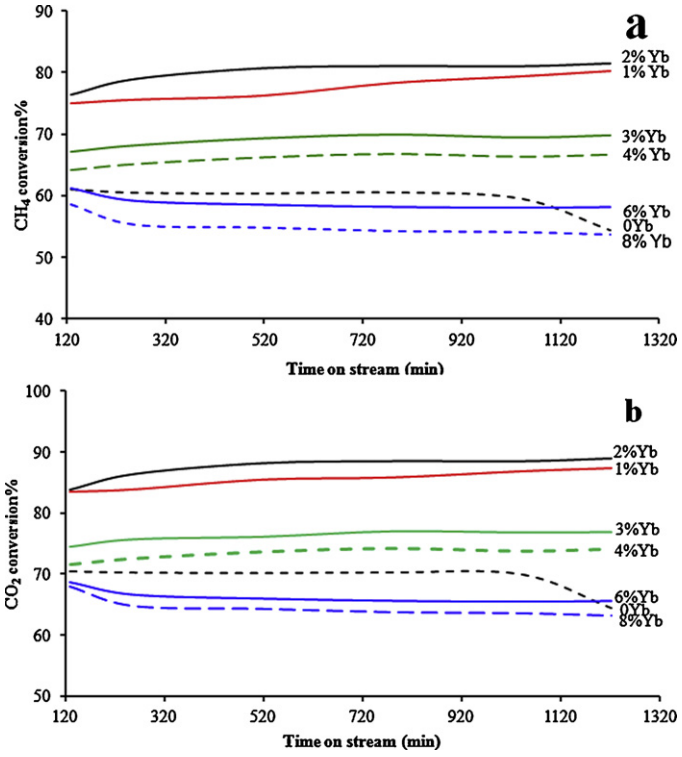

Fig. 7. Effect of Yb content (wt%) on the conversion of (a) CH_4 and (b) CO_2 over Ni/γ-Al_2O_3 catalysts (reaction conditions: reaction temperature = 700 °C; GHSV = 5.2×10^4 mL g^{-1} h^{-1}; CO_2:CH_4 = 1.0, TOS = 20 h).

20 h. The results, in terms of CH_4 and CO_2 conversion, from the aforementioned tests are presented in Fig. 7a and b. No data is reported during the initial 2 h in Fig. 7a and b due to all the materials being subjected to an in situ reduction step of 2 h duration prior to the introduction of the dry reforming reactant gases. From the results presented in Fig. 7a and b it can seen that the materials containing 1 and 2% Yb were clearly more active in terms of CH_4 and CO_2 conversion than all of the other materials tested. These materials were able to catalyse CH_4 conversions between 75 and 81.5% and CO_2 conversions between 83.5 and 89% throughout the entire testing period studied. The CH_4 conversion approached the conversion expected for the system at thermodynamic equilibrium which is 91.5% [63] (CH_4/CO_2 = 1, atmospheric pressure and 900 °C). Hence, as the CH_4 conversion expected under conditions of thermodynamic equilibrium was not obtained it was controlled by kinetics. The CO_2 conversion was higher than that expected if the system was at thermodynamic equilibrium (66.3%) [63], due to the influence of the RWGS (reverse water gas shift) reaction, which has been reported to occur under the experimental conditions described here [64–66].

$$CO_2 + H_2 \rightarrow CO + H_2O \quad \text{(RWGS)} \qquad (2)$$

Of the other Yb doped materials tested (3, 4, 6 and 8% Yb) the materials with the two highest Yb loadings (6 and 8%) were clearly less active then the materials with intermediate Yb loadings (3 and 4%), whilst the un-doped material achieved conversions similar to the material doped with 6% Yb. The trends observed in activity for the un-doped and Yb doped Ni/γ-Al_2O_3 materials correlated strongly with the average Ni particle sizes of these materials (Fig. 8) with the degree of CH_4 and CO_2 conversions observed increasing with decreasing average Ni particle size.

The H_2/CO ratios obtained at 520 min, as a function of catalyst Yb content, are shown in Fig. 9. From the data given in Fig. 9 it can be seen that the H_2/CO ratios were not one (as predicted based on the

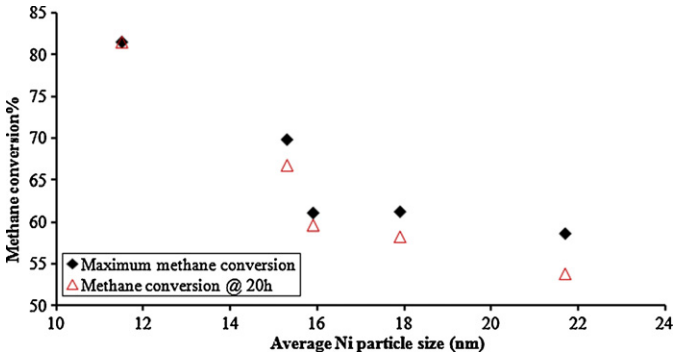

Fig. 8. CH_4 conversion versus average Ni particle size.

stoichiometry of the overall dry reforming reaction (reaction (1)). This however was expected as thermodynamics predicts a H_2/CO ratio of unity only at temperatures above 800 °C [67]. The H_2/CO ratios that were obtained have a similar pattern to the activity trends in terms of Yb% content. The un-doped Ni/γ-Al_2O_3 catalyst produced a product gas with a low H_2/CO ratio (0.90) which suggests the formation of steam due to the reverse water gas shift reaction [52], whilst the Ni/γ-Al_2O_3 catalysts containing 1 and 2% Yb respectively produced synthesis gas with the highest H_2/CO ratios of ~0.95. The improved H_2/CO ratio in the catalysts containing 1 and 2 wt% Yb was most likely due to reduced water gas shift reaction occurring. This in turn may have been due to more rapid conversion of CO_2 from improved active Ni surface area/particle size distribution and/or more active carbon. These aspects are discussed in detail in the later section.

In terms of stability all of the catalysts were relatively stable over the time frame tested (20 h) except for the un-doped material which had a significantly reduced activity after ~17 h. The significant loss of activity for this material was most likely due to excessive carbon deposition. The deposition of carbon is discussed in detail in the proceeding paragraphs.

The amount of carbon deposited on the spent catalysts (which is expressed in Table 5 in terms of carbon deposition rate) was determined using TGA. The TGA data showed that the carbon deposition rate was lowest when using the Ni-2Yb/γ-Al_2O_3 catalyst and highest when using the un-doped catalyst and the catalyst with the highest Yb loading. No clear trend in carbon deposition rate was observed for the materials tested. Interestingly the amount of carbon deposited on the un-doped catalyst, which underwent a significant loss in activity in terms of CO_2 conversion at ~17 h, was slightly lower than the amount deposited on the 8%Yb catalyst which displayed stable activity up to 20 h of testing. This result indicates that the amount of carbon deposited was either most likely not solely responsible for the significant loss of activity observed

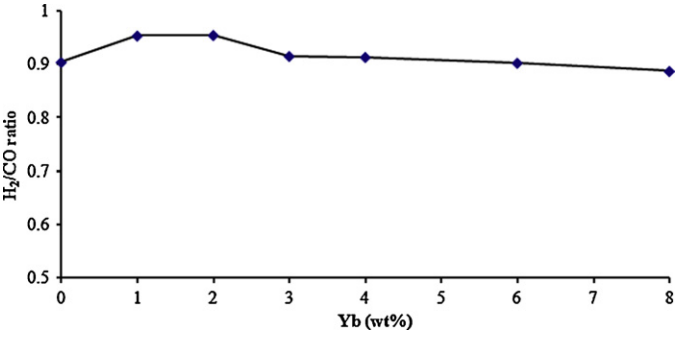

Fig. 9. Effect of Yb content (wt%) on the H_2/CO ratio at 520 min time on stream (reaction conditions: reaction temperature = 700 °C; GHSV = 5.2×10^4 mL g^{-1} h^{-1}; CO_2:CH_4 = 1.0).

Table 5
Rate of carbon deposition on spent Ni/γ-Al_2O_3 catalysts with different Yb loading.

Yb load (wt%)	0	2	4	6	8
Carbon deposition rate ($g_c\ g^{-1}{}_{cat.}\ h^{-1}$)	8.7×10^{-6}	1.3×10^{-7}	5.2×10^{-7}	5.1×10^{-7}	9.1×10^{-6}

Table 6
Ratio of Raman bands at 1290–1594 due to deposited carbon for spent catalysts and commercial single walled carbon nanotubes (SWCNTs).

Material	SWCNTs	Ni/γ-Al_2O_3	Ni-2Yb/γ-Al_2O_3	Ni-4Yb/γ-Al_2O_3	Ni-6Yb/γ-Al_2O_3	Ni-8Yb/γ-Al_2O_3
I_D/I_G ratio	0.25	1.73	1.50	1.85	1.94	1.93

and that it may have been due to the type(s) of carbon deposited and/or the location of the carbon deposition.

The type(s) of carbon deposited on the catalysts that were used in the dry reforming tests was investigated using a range of techniques (XRD, Raman Spectroscopy and TEM). XRD analysis of the spent catalysts (Fig. 10) revealed that they all contained graphitic carbon based on the presence of the strong peak observed at ~26.2° 2θ. According to the literature this peak was due to the graphite (0 0 2) lattice plane of carbon nanotubes [68]. The degree of graphitisation of the carbon deposited on the different spent catalysts was calculated using the Maire and Mering formula [69]:

$$d = 3.354 + 0.086(1 - g)$$

where d is the inter plane distance (d_{002}) in angstroms, and g is the percentage graphitisation.

Of the catalysts tested the Ni-2Yb/γ-Al_2O_3 showed the highest degree of graphitisation (0.60) compared to the 0, 4, 6 and 8 wt% Yb catalysts which had a similar degree of graphitisation of ~0.45. The higher degree of graphitisation of the carbon on the Ni-2Yb/γ-Al_2O_3 catalyst was most likely linked with the significantly lower amount of carbon that deposited on this catalyst compared to the other catalysts.

Raman spectroscopy was also used to investigate the type of carbon deposited on the spent catalysts. The results from these analyses are presented in Fig. 11 and Table 6. The Raman spectrum of single walled carbon nanotubes was also obtained for comparison and is presented in Fig. 11. The spectra obtained for all the spent catalysts showed bands at 1290 cm^{-1} (D band) and 1584 cm^{-1} (G band). The band at 1584 cm^{-1} corresponds to an E_{2g} vibration mode of graphite and is related to sp^2-bonded carbon atoms in a two dimensional hexagonal lattice, such as in a graphite layer [70]. Carbon nanotubes with concentric layers of hexagonal carbon lattice display the same vibration. The band at ~1290 cm^{-1} indicates disordered sp^2-hybridised carbon atoms. The relative intensity ratios of the D and G bands (I_D/I_G) of the spent catalysts are given in Table 6. The relative intensity ratio, I_D/I_G, can be used to express the graphitisation of carbon nanotubes or the degree of disorder in the structure (i.e. the quality of the carbon nanotubes). Tan et al. [71] reported values of I_D/I_G = 0.051 for highly oriented pyrolytic graphite (highly organised), I_D/I_G = 0.430 for carbon nanotubes prepared by dc arc discharge and I_D/I_G = 3.56 for carbon nanotubes prepared by catalytic methods. For the Ni-2Yb/γ-Al_2O_3 catalyst, I_D/I_G = 1.50, indicating that the carbon nanotubes deposited on this catalyst are more graphitised than those deposited on the other spent catalysts. This is also in good agreement with the extent of graphitisation determined using the XRD results.

TEM images obtained of the non-promoted and 2 wt% Yb promoted spent catalysts (Fig. 12) clearly show that a mixture of amorphous coke, carbon nano-fibres and carbon nanotubes formed on the non-promoted and 2 wt% Yb promoted Ni/γ-Al_2O_3 catalysts. This result is similar to that reported by Liu et al., where they found a few carbon nano-fibres and multi walled carbon nanotubes on a Zr-incorporated MCM-41 Ni-based catalyst [26]. From the images presented in Fig. 12 it can be seen that the Ni metal particles at the bottom of deposited carbon nano-fibres and nanotubes have a very similar size to the diameter of the deposited carbon. This is in agreement with earlier reports [37,72,73].

The TEM images obtained also show that the proportion of carbon deposited as nanotubes versus amorphous coke and carbon nano-fibres was significantly higher in the 2 wt% Yb promoted catalyst as compared to the non-doped catalyst, which is in agreement with the Raman results.

In addition, a few SWCNTs with average outer diameters of ~14 nm were observed on the 2 wt% Yb promoted spent catalyst (refer to inset Fig. 12). The presence of SWCNTs has not previously been reported.

It has been previously suggested that the existence of carbon nanotubes can enhance Ni catalysed carbon dioxide reforming of methane [74]. Hence the improved performance of the Ni-2Yb/γ-Al_2O_3 catalyst over the other materials tested may have been in part due to the increased proportion of carbon deposited on this catalyst in the form of carbon nanotubes.

The sizes of the Ni particles in the catalysts after testing were also investigated using XRD. The XRD results (Table 7) showed that the catalysts containing Yb did not undergo considerable levels of

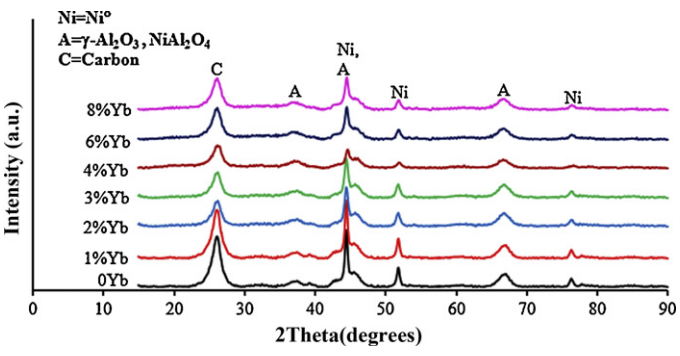

Fig. 10. XRD patterns of spent catalysts (after 20 h on stream at 700 °C).

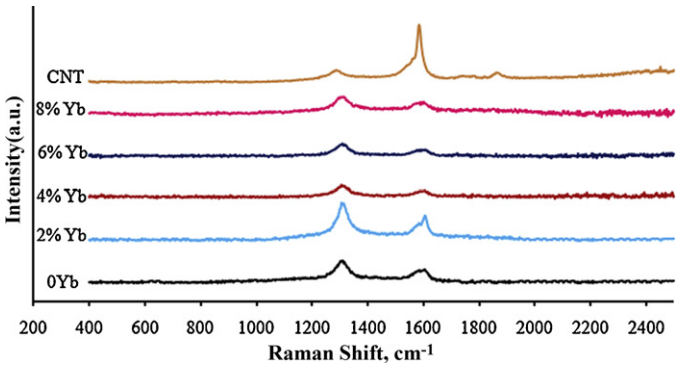

Fig. 11. Raman spectra of spent catalysts and single walled carbon nanotubes.

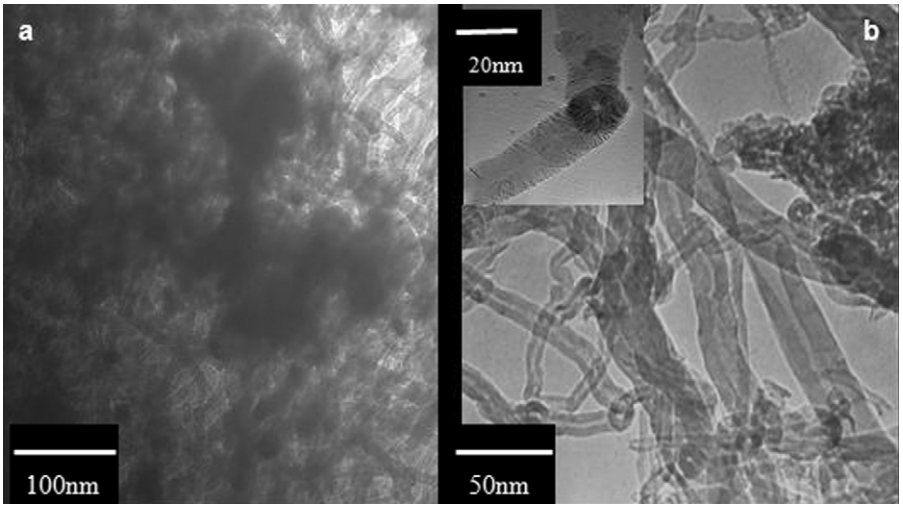

Fig. 12. Transmission electron micrographs of spent catalysts (a) Ni/γ-Al_2O_3 and (b) Ni-2Yb/γ-Al_2O_3. The inset in (b) shows a TEM image of an approximately 14 nm diameter SWCNT.

Table 7
Size of Ni particles in spent Ni/γ-Al_2O_3 catalysts with different Yb loading after 20 h time on stream.

Yb load (wt%)	0	2	4	6	8
Particle size[a] (nm)	18.0	11.4	15.1	17.5	19.7

[a] Measured by X-ray diffraction line broadening method and Scherrer formula.

Ni particle sintering during testing. The addition of Yb could prevent the tendency to Ni coarsening in the catalyst and increase the resistance to coking. However, the undoped Ni/γ-Al_2O_3 showed about 13% growth in the size of the particle. Resistance to sintering is an important issue of the reforming reaction of methane with carbon dioxide over nickel-based catalysts because the aggregation and sintering of the metal will reduces the total and metallic surface area and accelerate carbon deposition [7,20,37,75].

4. Discussion

The significant improvement in activity and stability of the Ni/γ-Al_2O_3 catalysts containing a low level of Yb (1–2 wt%) over the other catalysts tested in this study (non-doped and 4–8% Yb doped) was most likely due to a combination of factors. Previous studies on catalysed dry reforming of methane with Ni based catalysts have discussed numerous possible factors that can contribute to increased activity and stability. These factors include reducibility of metal oxide, metal particle size/distribution, amount and type of carbon deposited, coking rate and metal sintering. Based on the results obtained in this study the presence of low levels of Yb (1–2 wt%) contributed significantly to a number of the aforementioned factors. Firstly the addition of low levels of Yb enhanced the reducibility of the catalysts as shown by the TPR results. This enhanced reducibility was most likely due to either better-dispersion of Ni and/or an appropriate interaction between metal and support that led to an increase in the Ni reducibility [76]. In addition, the enhancement of the reducibility at lower temperature may have been due to the ability of Yb to increase the oxygen mobility within the bulk and suppression of the formation of an inactive $NiAl_2O_4$ phase, similar to the effect reported from the addition of Ce to Ni/Al_2O_3 catalysts [62,76,77]. Similarly, many studies have shown that the addition of other promoters such as Pd [37], Pt [36], K [44] and La [76] can increase the catalytic activity by enhancing the reducibility of the catalysts.

It has been demonstrated that the net formation of carbon on Ni-based catalysts is connected with the Ni particle size [37]. It was reported that the smaller Ni particles are able to suppress carbon deposition due to the "size effect", as opposite to the large nickel clusters which are prone to carbon deposition [37,78,79]. In contrary others have reported that a decrease in Ni particle size resulted in a larger amount of coke formation over Ni [80]. The influence of low levels of Yb on Ni particle size/particle size distribution also most likely had a significant role in the increased activity observed for the Ni-2Yb/γ-Al_2O_3 catalyst. The smaller average particle size in the aforementioned catalyst (Table 1) (combined with its high percentage of Ni surface atoms) would have led to increased active metal surface area in this catalyst which in turn would have led to increased activity. The particle size distribution of this catalyst also most likely had a significant role in the amount and kind of carbonaceous species' deposited [4,7,15,20,37,50,81–88]. It has been reported that in the reforming reaction various types of carbon, with different morphology, can form such as adsorbed atomic carbon (carbidic carbon) [54,81], amorphous carbon (moss-like and coke) [20,24,44,49,52,58,74,81,82,37,86–92], films (shell-like) [54,37], filamentous carbon (whisker-like) [20,37,38,44,47,54,77,81,86], and carbon nanotubes [35,54].

Based on the particle size distribution obtained for the Ni-2Yb/γ-Al_2O_3 catalyst (as compared to the other catalysts tested) and the differences in deposited carbon on this catalyst compared to the other catalysts tested (reduced overall amount of carbon and higher of graphitised carbon) the optimum Ni particle size range for reduced carbon deposition and/or formation of active carbon is 6–20 nm. The influence of Ni particles <6 nm is difficult to determine with a high degree of confidence based on the results obtained as the activity observed versus proportion of particles in this size range did not follow a definitive trend (Fig. 4) (although the most active catalyst did have the lowest proportion of particles in this size range). It is possible that Ni particles smaller than 5 nm lead to formation of carbon nano-fibres with outer diameters less than 5 nm (see Fig. 12a), and that these fibres cannot be readily gasified with CO_2, which in turn may deactivate the catalysts by covering these Ni particles. Based on the results obtained Ni particles >20 nm also most likely lead to increased carbon deposition/formation of carbon with reduced reactivity. This is consistent with previous studies that report that Ni particles >20 nm lead to formation of amorphous carbon which cannot easily be eliminated by gasification with CO_2. Amorphous carbon has also been

reported to encapsulate Ni particles, causing catalyst deactivation [20,37,54,86,87].

This result agrees with those in the reports that revealed the CNTs on the promoted Ni/γ-Al_2O_3 catalysts could be eliminated readily [7,85] and also suggested that the existence of CNTs can enhance Ni catalysed carbon dioxide reforming of methane [74]. This would be related to the location of the Ni particle with respect to the deposited carbon [37], where a significant amount of the metallic Ni particles could be located on the tip of CNTs, and that these may catalyse CH_4 decomposition [93]. Instead of nano-fibres that Ni metal particles were at the bottom of the fibres, Ni particles were located at the top of the CNTs, which can also be used as active sites for methane reforming [7]. This result is similar to the work reported by Gohier et al. [89] where they found that the growth mode switches from "tip-growth" for large particles ($\gg$5 nm) to "base-growth" for smaller ones (<5 nm). This behaviour had been earlier mentioned in other reports that CNTs grown from their base whilst carbon nano-fibres are shown to follow the tip-growth mode [90–92].

5. Conclusions

In summary, the introduction of 2 wt% Yb as promoter to the Ni(20 wt%)/γ-Al_2O_3 catalyst via sol–gel method leads to superior catalytic activities and stabilities. The addition of small amounts of Yb_2O_3 significantly improved the stability and dispersion of active nickel component. The reduction temperature for nickel on 2 wt% Yb-loaded-γ-Al_2O_3 catalyst was decreased compared to the catalysts without Yb. The catalyst displayed a significant enhancement in the CH_4 (about 33%) and CO_2 (about 27%) conversion. The addition of higher amount of ytterbium resulted in a decrease in catalytic activity due to the blockage of active sites by excess amounts of deposited carbon. Amongst the examined pure and Yb doped catalysts, the prevention of deactivation and degree of graphitisation was observed most in the case of sol–gel prepared 2 wt% Yb-doped Ni/γ-Al_2O_3 catalyst. CH_4 decomposition on the homogeneous Ni^0 particle size distribution between 6 and 20 nm was found to be the optimum which produces a higher proportion of tip-growth CNTs and provides Ni particles at the top of the CNTs, which can act as active sites for methane reforming. The existence of SWCNTs also enhanced the performance of Ni particles towards catalysing the CO_2 reforming of methane.

Acknowledgements

This work was supported by ARC Discovery (DP0881773). KM and JN gratefully acknowledge the ARC Discovery for postdoctoral fellowship and APA for the doctoral fellowship, respectively. Authors acknowledge Dr. Samuel Ippolito for his help in making the reactor system automated.

References

[1] L. Xu, H. Song, L. Chou, Appl. Catal., B 108–109 (2011) 177–190.
[2] S. Corthals, J.V. Nederkassel, H.D. Winne, J. Geboers, P. Jacobs, B. Sels, Appl. Catal., B 105 (2011) 263–275.
[3] Y. Ma, Y. Xu, M. Demura, T. Hirano, Appl. Catal., B 80 (2008) 15–23.
[4] L. Pino, A. Vita, F. Cipiti, M. Lagana, V. Recupero, Appl. Catal., B 104 (2011) 64–73.
[5] S. Lee, G. Keskar, C. Liu, W.R. Schwartz, C.S. McEnally, J. Kim, L.D. Pfefferle, G.L. Haller, Appl. Catal., B 111–112 (2012) 157–164.
[6] J. Guo, H. Lou, X. Zheng, Carbon 45 (2007) 1314–1321.
[7] X. Junke, Z. Wei, W. Jihui, L. Zhaojing, M. Jianxin, Chin. J. Catal. 30 (11) (2009) 1076–1084.
[8] F. Barrai, T. Jackson, N. Whitmore, M.J. Castaldi, Catal. Today 129 (2007) 391–396.
[9] L. Guczi, G. Stefler, O. Geszti, I. Sajo, Z. Paszti, A. Tompos, Z. Schay, Appl. Catal., A 375 (2010) 236–246.
[10] S. Seok, S.H. Choi, E.D. Park, S.H. Han, J.S. Lee, J. Catal. 209 (1) (2002) 6–15.
[11] M.M. Barroso-Quiroga, A.E. Castro-Luna, Int. J. Hydrogen Energy 35 (2010) 6052–6056.
[12] Z. Cheng, Q. Wu, J. Li, Q. Zhu, Catal. Today 30 (1–3) (1996) 147–155.
[13] K. Takanabe, K. Nagaoka, K. Nariai, K. Aika, J. Catal. 232 (2005) 268–275.
[14] K. Opoku-Gyamfi, Z.M. Tafreshi, A.A. Adesina, React. Kinet. Catal. Lett. 64 (2) (1998) 229–238.
[15] J. Zhang, H. Wang, A.K. Dalai, J. Catal. 249 (2) (2007) 300–310.
[16] A.E.C. Luna, M.E. Iriarte, Appl. Catal., A 343 (1–2) (2008) 10–15.
[17] V. García, J.J. Fernández, W. Ruíz, F. Mondragón, A. Moreno, Catal. Commun. 11 (4) (2009) 240–246.
[18] K.Y. Koo, H.S. Roh, U.H. Jung, D.J. Seo, Y.S. Seo, W.L. Yoon, Catal. Today 146 (2009) 166–171.
[19] S. Therdthianwong, A. Therdthianwong, C. Siangchin, S. Yongprapat, Int. J. Hydrogen Energy 33 (3) (2008) 991–999.
[20] R. Yang, C. Xing, C. Lv, L. Shi, N. Tsubaki, Appl. Catal., A 385 (2010) 92–100.
[21] C.E. Daza, J. Gallego, F. Mondragón, S. Moreno, R. Molina, Fuel 89 (3) (2010) 592–603.
[22] F. Pompeo, D. Gazzoli, N.N. Nichio, Int. J. Hydrogen Energy 34 (2009) 2260–2268.
[23] A. Nandini, K.K. Pant, S.C. Dhingra, Appl. Catal., A 290 (2005) 166–174.
[24] H. Jeong, K.I. Kim, D. Kim, I.K. Song, J. Mol. Catal. A: Chem. 246 (1–2) (2006) 43–48.
[25] S.H. Seok, S.H. Han, J.S. Lee, Appl. Catal., A 215 (1–2) (2001) 31–38.
[26] D. Liu, X.Y. Quek, W.N. Cheo, R. Lau, A. Borgna, Y. Yang, J. Catal. 266 (2009) 380–390.
[27] H.W. Chen, C.Y. Wang, C.H. Yu, L.T. Tseng, P.H. Liao, Catal. Today 97 (2004) 173–180.
[28] D. Halliche, R. Bouarab, O. Cherifi, M.M. Bettahar, Catal. Today 29 (1–4) (1996) 373–377.
[29] J.X. Wang, Y. Liu, T.X. Cheng, W.X. Li, Y.L. Bi, K.J. Zhen, Appl. Catal., A 250 (1, 10) (2003) 13–23.
[30] M.S. Fan, A. Zuhairi Abdullah, S. Bhatia, Appl. Catal., B 100 (2010) 365–377.
[31] A. Valentini, N.L.V. Carreño, L.F.D. Probst, P.N. Lisboa-Filho, W.H. Schreiner, E.R. Leite, E. Longo, Appl. Catal., A 255 (2, 8) (2003) 211–220.
[32] W. Nimwattanakul, A. Luengnaruemitchai, S. Jitkarnka, Int. J. Hydrogen Energy 31 (1) (2006) 93–100.
[33] T.C. Xiao, T. Suhartanto, A.P.E. York, J. Sloan, M.L.H. Green, Appl. Catal., A 253 (2003) 225–235.
[34] S. Therdthianwong, C. Siangchin, A. Therdthianwong, Fuel Process. Technol. 89 (2008) 160–168.
[35] M. García-Diéguez, E. Finocchio, M.A. Larrubia, L.J. Alemany, G. Busca, J. Catal. 274 (2010) 11–20.
[36] M. García-Diéguez, I.S. Pieta, M.C. Herrera, M.A. Larrubia, L.J. Alemany, J. Catal. 270 (2010) 136–145.
[37] S. Damyanova, B. Pawelec, K. Arishtirova, J.L.G. Fierro, C. Sener, T. Dogu, Appl. Catal., B 92 (2009) 250–261.
[38] H. Arbag, S. Yasyerli, N. Yasyerli, G. Dogu, Int. J. Hydrogen Energy 35 (2010) 2296–2304.
[39] B. Pawelec, S. Damyanova, K. Arishtirova, J.L.G. Fierro, L. Petrov, Appl. Catal., A 323 (2007) 188–201.
[40] T. Horiuchi, K. Sakuma, T. Fukui, Y. Kubo, T. Osaki, T. Mori, Appl. Catal., A 144 (1996) 111–120.
[41] J.S. Chang, S.E. Park, H. Chon, Appl. Catal., A 145 (1–2) (1996) 111–120.
[42] F. Frusteri, F. Arena, G. Calogero, T. Torre, A. Parmaliana, Catal. Commun. 2 (2) (2001) 49–56.
[43] F. Frusteri, L. Spadaro, F. Arena, A. Chuvilin, Carbon 40 (7) (2002) 1063–1070.
[44] J. Juan-Juan, M.C. Roman-Martinez, M.J. Illan-Gomez, Appl. Catal., A 301 (1) (2006) 9–15.
[45] Z.L. Zhang, X.E. Verykios, Catal. Today 21 (2–3) (1994) 589–595.
[46] J.A.C. Dias, J.M. Assaf, Catal. Today 85 (1) (2003) 59–68.
[47] M. Ocsachoque, F. Pompeo, G. Gonzalez, Catal. Today 172 (2011) 226–231.
[48] N. Laosiripojana, W. Sutthisripok, S. Assabumrungrat, Chem. Eng. J. 112 (1–3) (2005) 13–22.
[49] W.D. Zhang, B.S. Liu, C. Zhu, Y.L. Tian, Appl. Catal., A 292 (2005) 138–143.
[50] S. Wang, G.Q. Lu, Appl. Catal., B 19 (3–4) (1998) 267–277.
[51] Z.W. Liu, H.S. Roh, K.W. Jun, J. Ind. Eng. Chem. 9 (3) (2003) 267–274.
[52] C.E. Daza, S. Moreno, R. Molina, Int. J. Hydrogen Energy 36 (2011) 3886–3894.
[53] R.G. Ding, Z.F. Yan, Catal. Today 68 (1–3) (2001) 135–143.
[54] A. Horváth, G. Stefler, O. Geszti, A. Kienneman, A. Pietraszek, L. Guczi, Catal. Today 169 (1) (2011) 102–111.
[55] M.H. Amin, K. Mantri, S.K. Bhargava, Proc. Chemeca 2010, The University of Adelaide, Australia, September 2010.
[56] Q. Liang, L.z. Gao, Q. Li, S.H. Tang, B.C. Liu, Z.L. Yu, Carbon 39 (2001) 897–903.
[57] S.Y. Foo, C. Cheng, T.H. Nguyen, A.A. Adesina, Catal. Today 164 (1) (2011) 221–226.
[58] K. Zhang, G. Zhou, J. Li, T. Cheng, Catal. Commun. 10 (2009) 1816–1820.
[59] M. Ozawa, M. Kimura, J. Mater. Sci. Lett. 9 (3) (1990) 291–293.
[60] M. Ozawa, M. Kimura, A. Isogai, J. Mater. Sci. Lett. 9 (1990) 709–711.
[61] B.S. Liu, C.T. Au, Appl. Catal., A 244 (2003) 181–195.
[62] H. Li, H. Xu, J. Wang, J. Nat. Gas Chem. 20 (2011) 1–8.
[63] M. Khoshtinat Nikoo, N.A.S. Amin, Fuel Process. Technol. 92 (2011) 678–691.
[64] C. Shi, P. Zhang, Appl. Catal., B 115–116 (2012) 190–200.
[65] M.M.V.M. Souza, D.A.G. Aranda, M. Schmal, J. Catal. 204 (2001) 498–511.
[66] N. Laosiripojana, S. Assabumrungrat, Appl. Catal., B 60 (2005) 107–116.
[67] S. Damyanova, B. Pawelec, K. Arishtirova, M.V.M. Huerta, J.L.G. Fierro, Appl. Catal., B 89 (2009) 149–159.

[68] A.S. Ferlauto, D.Z. de Florio, F.C. Fonseca, V. Esposito, R. Muccillo, E. Traversa, L.O. Ladeira, Appl. Phys. A: Mater. Sci. Process. 84 (3) (2006) 271–276.
[69] J. Yan, L.F. Yi, W.R. Zhong, J. Serb. Chem. Soc. 70 (2) (2005) 277–282.
[70] F. Tuinstra, J.L. Koening, J. Chem. Phys. 53 (3) (1970) 1126–1131.
[71] P. Tan, S. Zhang, K. To Yue, F. Huang, J. Raman Spectrosc. 28 (1997) 369–372.
[72] J. Ashok, S.N. Kumar, A. Venugopal, V.D. Kumari, M. Subrahmanyam, J. Power Sources 164 (2007) 809–814.
[73] K. Otsuka, H. Ogihara, S. Takenaka, Carbon 41 (2003) 223–233.
[74] Y. Qu, A.M. Sutherland, T. Guo, Energy Fuels 22 (2008) 2183–2187.
[75] L. Ji, S. Tang, H.C. Zeng, J. Lin, K.L. Tan, Appl. Catal., A 207 (2001) 247–255.
[76] P. Kumar, Y. Sun, R.O. Idem, Energy Fuels 22 (2008) 3575–3582.
[77] A. Piras, A. Trovarelli, G. Dolcetti, Appl. Catal., B 28 (2000) L77–L81.
[78] S. Sokolov, E.V. Kondratenko, M.M. Pohl, A. Barkschat, U. Rodemerck, Appl. Catal., B 113–114 (2012) 19–30.
[79] T. Osaki, T. Mori, J. Catal. 204 (2001) 89–97.
[80] X.Y. Quek, D. Liu, W.N.E. Cheo, H. Wang, Y. Chen, Y. Yang, Appl. Catal., B 95 (2010) 374–382.
[81] J.H. Kim, D.J. Suh, T.J. Park, K.L. Kim, Appl. Catal., A 197 (2000) 191–200.
[82] S. Tang, L. Ji, J. Lin, H.C. Zeng, K.L. Tan, K. Li, J. Catal. 194 (2000) 424–430.
[83] D. Chen, R. Lodeng, A. Anundskas, O. Olsvik, A. Holmen, Chem. Eng. Sci. 56 (2001) 1371–1379.
[84] V.C.H. Kroll, H.M. Swaan, C. Mirodatos, J. Catal. 161 (1996) 409–422.
[85] X. Jun-Ke, L. Zhao-Jing, W. Ji-Hui, Z. Wei, M. Jian-Xin, Acta Phys.-Chim. Sin. 25 (02) (2009) 253–260.
[86] X. Zhu, P. Huo, Y. Zhang, D. Cheng, C. Liu, Appl. Catal., B 81 (2008) 132–140.
[87] M. Matsukata, T. Matsushita, K. Ueyama, Energy Fuels 9 (1995) 822–828.
[88] F. Danafar, A. Fakhrul-Razi, M.A.M. Salleh, D.R.A. Biak, Chem. Eng. Res. Des. 89 (2011) 214–223.
[89] A. Gohier, C.P. Ewels, T.M. Minea, M.A. Djouadi, Carbon 46 (2008) 1331–1338.
[90] L. Delzeit, I. McAninch, B.A. Cruden, D. Hash, B. Chen, J. Han, J. Appl. Phys. 91 (9) (2002) 6027–6033.
[91] S. Hofmann, R. Sharma, C. Ducati, G. Du, C. Mattevi, C. Cepek, Nano Lett. 7 (3) (2007) 602–608.
[92] M. Lin, J.P.Y. Tan, C. Boothroyd, K.P. Loh, E.S. Tok, Y.L. Foo, Nano Lett. 7 (8) (2007) 2234–2238.
[93] R.M. Navarro, M.A. Pena, J.L.G. Fierro, Chem. Rev. 107 (2007) 3952–3991.